

Paper:

Two-Dimensional Wireless Power Supply to Ubiquitous Robots Using Microwaves

Hiroyuki Shinoda^{*1}, Yasutoshi Makino^{*2}, Naoshi Yamahira^{*3}, and Hiroto Itai^{*4}

^{*1}The University of Tokyo

7-3-1 Hongo, Bunkyo-ku, Tokyo 113-8656, Japan

E-mail: shino@alab.t.u-tokyo.ac.jp

^{*2}Keio University

^{*3}JFE Steel Corporation

^{*4}Cellcross Co. Ltd.

[Received January 18, 2010; accepted January 28, 2010]

This paper proposes a wireless power supply method to ubiquitous small robots using microwaves propagated in a two-dimensional waveguide (2DW). A robot working anywhere on a 2DW sheet receives the power from the sheet. The communication signal is also transmitted through the identical sheet. The structure of 2DW sheet is simple and realized with various materials at low cost. Since the microwave power is confined inside the 2DW sheet, it enables safe power transmission and communication without strong interference with the space outside the sheet.

Keywords: wireless power transmission, ubiquitous robot, ambient mechatronics, surface LAN, two-dimensional communication

1. Introduction

Ubiquitous small robots have great potential for supporting our everyday activities [1]. They can keep the environment clean and tidy and watch people for timely assistance both in homes and public spaces. A crucial problem for practical use of such robots is the power supply to the robots. Since charging the batteries by hand is not acceptable in practical scenes, wireless power transmission is desired for expanding the possibility.

Current wireless power transmission technology is classified into three types: conventional induction coupling [2], electromagnetic wave connection [3], and recently proposed resonant coupling [4]. In the inductive coupling method, a coupling coil located under a robot supplies the power to the robot. Thus large scale coil arrays over floors and walls are necessary for powering ubiquitous robots. On the other hand, the methods based on electromagnetic wave connection and resonant coupling provide the freedom of the robot location relative to the power source. Instead, strong electromagnetic fields are produced around the robots working with people, which poses a considerable problem of electromagnetic compatibility (EMC).

The fourth possibility, which we propose, is a power

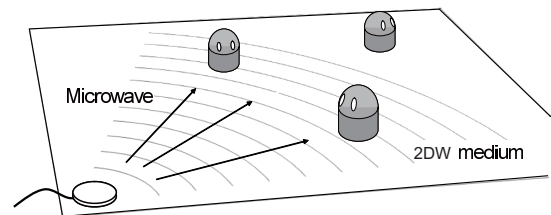


Fig. 1. Powering small ubiquitous robots using a 2DW medium. Power supplied to individual robots is assumed to be ≤ 1 W in the present system.

supply using two-dimensional waveguide (2DW) shown in Fig. 1. Robots working on the sheet receive power and exchange signals through electromagnetic waves propagating in a thin 2DW sheet. Power to a robot is assumed to be less than 1 W in the present system. The structure of the 2DW sheet is simple and implemented at low cost on large areas of walls and floors. Since the 2DW sheet confines microwave power, it enables safe power transmission and communication without strong interference with the space outside the sheet.

The concept of 2DW system using microwaves has been reported since 2006 [5–7]. Some commercial products for signal transmission and RFID-tag reading have already been available as LAN Sheet and @CELL RFID. In the previous reports, however, no application to ubiquitous robots was mentioned and the power transmission mechanism was not fully disclosed. We move beyond the previous reports to demonstrate the basic principle of 2D power transmission and the experimental results.

2. Non-Contact Connection to 2DW Sheet

Figure 2 shows two possible types of 2DW which trap microwaves and provide nearby robots with power through couplers. In this paper, we assume using a frequency band of 2.4–2.5 GHz, called Industry-Science-Medical (ISM) band based on the following reason. Assuming that a ubiquitous robot uses a coupler 10 cm square, it should use a microwavelength less than 10 cm

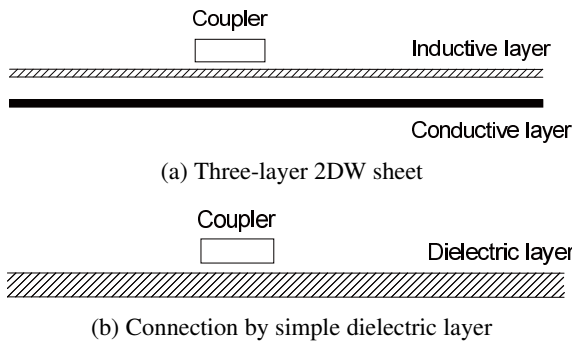


Fig. 2. Cross-sections of possible 2DW sheets. (a) is studied in this work.

for highly efficient power transmission using convergent waves. For relative dielectric constant $\epsilon_r = 1.5$ of the medium, the 10 cm wavelength corresponds to a frequency of 2.4 GHz, which means that the frequency used should be ≥ 2.4 GHz. From the aspects of the transmission loss and robustness of the nearfield connection, we should minimize the frequency, which leads to the conclusion that we should use 2.4 GHz.

Assume ISM band to be used, the 2DW sheet in **Fig. 2(b)** cannot be used because it does not confine electromagnetic waves sufficiently. Most electromagnetic power runs along the surface outside the sheet thinner than the wavelength, with leakage typically reaching ≥ 10 cm in its height from the sheet surface, which may adversely affect the surroundings, including human beings.

In contrast, the 2DW in **Fig. 2(a)** has minimal leakage outside the sheet, maintaining high-efficiency connection using an especially designed resonance coupler.

2.1. Electromagnetic Wave Around 2DW Sheet

Within the coordinates in **Fig. 3**, the z component of the electric field above the sheet surface is written as follows:

$$E_z = \frac{k_2^2}{k_1} V \exp(-k_1 z) \exp(-jkx) \exp(j\omega t) \quad (z > 0) \quad (1)$$

$$\left(\begin{array}{l} k_1^2 = (\mu\epsilon - \mu_0\epsilon_0)\omega^2 - \frac{jZ\epsilon\omega}{h} \\ k_2^2 = \frac{jZ\epsilon\omega}{h} \\ k^2 = \mu\epsilon\omega^2 - \frac{jZ\epsilon\omega}{h} \end{array} \right)$$

using $j = \sqrt{-1}$, for the wave traveling toward $+x$, where μ is the sheet’s magnetic permeability, ϵ its dielectric constant, μ_0 the atmospheric magnetic permeability, ϵ_0 its dielectric constant, and parameter V voltage between top layer S and bottom layer B at $x = t = 0$. The Eq. (1) is an approximation assuming $|k_1 h| \ll 1$ and $|k_2 h| \ll 1$, where h is dielectric layer thickness.

Parameter Z is the sheet impedance of the top layer defined as follows:

$$Z \equiv R + jX \equiv \frac{E_x}{i_x} [\Omega] \quad \dots \quad (2)$$

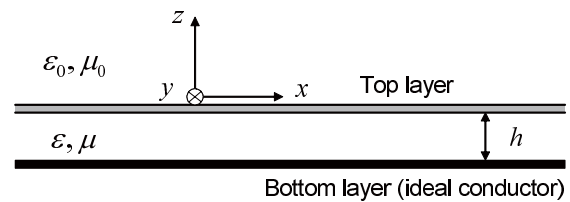


Fig. 3. Coordinates and sheet parameters.

E_x is electric field [V/m] along the x -axis at top layer S, i_x is current density [A/m] along the x -axis at the same layer, bottom layer B an ideal conductor, and top layer S sufficiently thin. If top layer S is an ideal continuous conductor, Z equals 0, yielding $E_x = 0$. A top layer whose sheet impedance is inductive as $X > 0$ is called an “inductive layer,” realized by a conductive mesh with a period shorter than the wavelength. When S is a mesh whose period is shorter than the wavelength, E_x and i_x are their averages within this period. We can easily confirm that the solution of Eq. (1) satisfies Maxwell’s equations [8].

Based on Eq. (1), we calculate leakage ratio r defined as the ratio of electromagnetic energy flow J_1 running in the $+x$ direction outside of the sheet to energy flow J_2 inside the sheet:

$$r \equiv \frac{J_1}{J_2} = \frac{\pi\epsilon_0}{\epsilon} \frac{\gamma^2}{\sqrt{1+\gamma^2}} h \sqrt{\frac{1}{\lambda^2} - \frac{1}{\lambda_0^2}} \quad \dots \quad (3)$$

λ_0 and λ are equal to the electromagnetic wavelength in air and that in a medium with ϵ and μ . Dimensionless parameter γ is defined as follows:

$$\gamma \equiv X \frac{\epsilon}{h(\epsilon\mu - \epsilon_0\mu_0)\omega} \quad \dots \quad (4)$$

i.e., normalized sheet inductance determining electromagnetic leakage and connection. If $\epsilon/\epsilon_0 = 1.4$, $\mu = \mu_0$, $h = 1$ mm, and $\gamma = 1.0$, r is 0.4% at 2.4 GHz. Electromagnetic waves are sent to or absorbed from the 2DW sheet when a conductive plate is placed near S, as explained later, while electromagnetic energy outside the sheet remains small without conductive or dielectric objects near the sheet.

2.2. Nearfield Connection

Assume conductive plate P is placed near the sheet where an electromagnetic wave runs in the $+x$ direction as shown in **Fig. 4**. Let 2DW sheet thickness be h , dielectric constant ϵ_2 , and μ_2 magnetic permeability inside sheet ($0 < z < h$). A dielectric layer with thickness H , dielectric constant ϵ_1 , and magnetic permeability μ_1 exists under P.

Solving Maxwell’s equations in $x > 0$ yields two modes running in the $+x$ direction as follows.

In two extreme cases as

- (i) $\left| j\omega X \left(\frac{\epsilon_1}{H} + \frac{\epsilon_2}{h} \right) \right| \gg |A|$
- (ii) $\left| j\omega X \left(\frac{\epsilon_1}{H} + \frac{\epsilon_2}{h} \right) \right| \ll |A|$

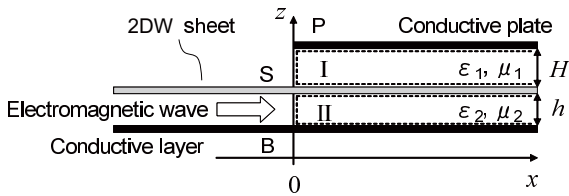


Fig. 4. Simple coupler consisting of a conductive plate and a dielectric layer. Electromagnetic energy between S and B is absorbed in the space between S and P.

mode expressions are simplified, where $A \equiv (\mu_2 \epsilon_2 - \mu_1 \epsilon_1) \omega^2$.

In this paper, we utilize the modes in case (i) which are written as follows.

Mode (a):

$$\begin{pmatrix} E_z^I \\ B_y^I \\ E_z^{II} \\ B_y^{II} \end{pmatrix} \approx C \begin{pmatrix} \frac{1}{\epsilon_1} \\ -\frac{\mu_1 \omega}{k_a} \\ \frac{1}{\epsilon_2} \\ -\frac{\mu_2 \omega}{k_a} \end{pmatrix} \exp(-jk_a x) \dots (5)$$

$$\left(k_a^2 = \frac{1}{\epsilon_1/H + \epsilon_2/h} \left(\frac{\epsilon_1}{H} \mu_2 \epsilon_2 + \frac{\epsilon_2}{h} \mu_1 \epsilon_1 \right) \omega^2 \right)$$

Mode (b):

$$\begin{pmatrix} E_z^I \\ B_y^I \\ E_z^{II} \\ B_y^{II} \end{pmatrix} \approx C \begin{pmatrix} -\frac{1}{H} \\ \frac{\epsilon_1 \mu_1 \omega}{k_b} \frac{1}{H} \\ \frac{1}{h} \\ -\frac{\epsilon_2 \mu_2 \omega}{k_b} \frac{1}{h} \end{pmatrix} \exp(-jk_b x) \dots (6)$$

$$\left(k_b^2 \approx \omega X \left(\frac{\epsilon_1}{H} + \frac{\epsilon_2}{h} \right) + \mu_1 \epsilon_1 \omega^2 \right)$$

E_z^I and E_z^{II} are z components of the electric field inside and outside the 2DW sheet. B_y^I and B_y^{II} are y components of magnetic flux density inside and outside the 2DW sheet, and C is a constant.

In derivation, we assume that electromagnetic field variation along z is small, equivalent to

$$\sqrt{\omega X \left(\frac{\epsilon_1}{H} + \frac{\epsilon_2}{h} \right)} H \ll 1 \text{ and } \sqrt{\omega X \left(\frac{\epsilon_1}{H} + \frac{\epsilon_2}{h} \right)} h \ll 1.$$

Since the wavenumber of Mode (a) k_a and that of Mode (b) k_b differ, they produce a beat along x with a period of

$$L = \frac{2\pi}{|k_a - k_b|} \dots (7)$$

An electromagnetic wave runs in the +x direction weaving between regions II ($0 < z < h$) and I ($h < z < h + H$) with period L. If we assume

$$\begin{pmatrix} E_z^I \\ E_z^{II} \end{pmatrix} = \begin{pmatrix} 0 \\ p \end{pmatrix} \dots (8)$$

at $x = 0$, we obtain the solution in $x > 0$ as

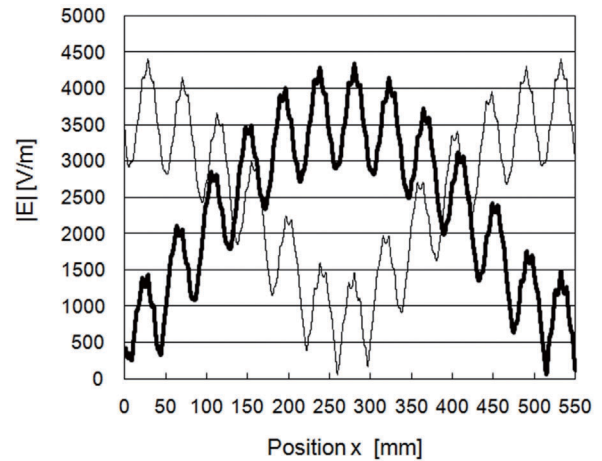


Fig. 5. Simulation results. Thick line: absolute electric field in region II. Thin line: absolute electric field in region I.

$$\begin{pmatrix} E_z^I \\ E_z^{II} \end{pmatrix} = p \left[\begin{pmatrix} \frac{1}{\epsilon_1/\epsilon_2 + H/h} \\ \frac{1}{1 + \epsilon_2 H / (\epsilon_1 h)} \end{pmatrix} \exp(jk_a x) + \begin{pmatrix} -\frac{1}{\epsilon_1/\epsilon_2 + H/h} \\ \frac{1}{1 + \epsilon_1 h / (\epsilon_2 H)} \end{pmatrix} \exp(jk_b x) \right] \dots (9)$$

When

$$\left| \frac{1}{1 + \epsilon_2 H / (\epsilon_1 h)} \right| = \left| \frac{1}{1 + \epsilon_1 h / (\epsilon_2 H)} \right|$$

that is,

$$\frac{H}{\epsilon_1} = \frac{h}{\epsilon_2} \dots (10)$$

there exist points at which the electric field becomes 0 inside the 2DW sheet (region II). In case difference $|k_a - k_b|$ is much smaller than $|k_a|$ and $|k_b|$, electromagnetic energy density vanishes at the zero points, meaning electromagnetic power is completely absorbed in region I out of the 2DW sheet. Length L is called the power exchange length, so a conductive plate larger than L absorbs all incident energy from the sheet in a 2D problem setting, as simulated in Fig. 5. The bold line shows the absolute electric field in region II and the thin line that in region I. Parameters are set to $\epsilon_1 = \epsilon_2 = 1.5\epsilon_0$ and $H = h = 2$ mm. The inductive layer is a mesh at 7 mm intervals with 1 mm line width. The power exchange length is 270 mm. The high-frequency fluctuations in the 42 mm period come from numerical simulation imperfectness. Waves in regions I and II are partially reflected at the right end of the simulation model.

For power transmission not powering unwanted objects, L should be maximized while maintaining the coupler connection to the 2DW sheet. To make connection between special couplers and the 2DW sheet efficient, couplers use resonance as detailed below.

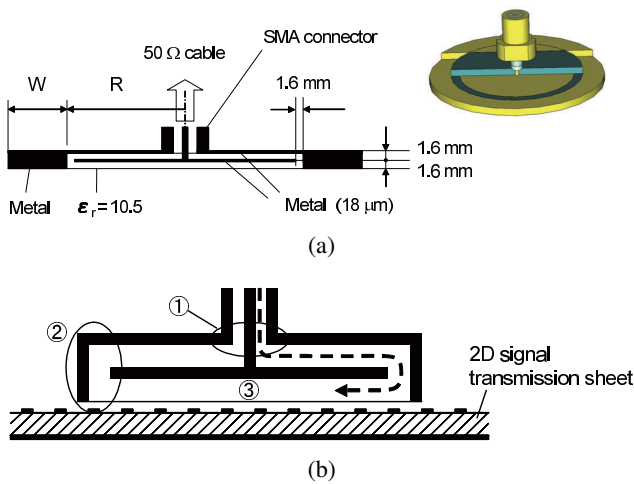


Fig. 6. Example of nearfield coupler design. (a) Axisymmetric coupler details and (b) principle illustrated.

2.3. Nearfield Coupler Design

An example of design concept on 2DW-based nearfield coupler is explained in **Fig. 6**. Connection assumes electromagnetic flow from the coupler cable to the sheet. Receiving efficiency is given by the reciprocity theorem. Putting the coupler on the 2DW sheet causes microwave from the coaxial cable to follow the winding axisymmetric path shown by the broken-line arrow. Reflections occur at ①, ②, and ③ in the coupler due to discontinuous impedance change. The reflected signal back to the coaxial cable is the mixture of the reflected signals at each point. Choosing coupler radius R to cancel the reflected signals, we reduce the reflected power. Ideally, the input signal is fed to the sheet without reflection back to the cable. In other words, we transfer power from the cable to the 2DW sheet using resonance. Even if coupler radius R is smaller than power exchange length L , input power is transferred to the 2DW sheet repeating reflections in the coupler. Practically, ohmic and dielectric loss in the coupler and radiation loss from the gap between the coupler and the sheet are considerable. Thus reducing them is a key in the future coupler design.

3. Simulations and Results

To confirm the above points, we modeled the 2DW sheet using MW-Studio software (AET Japan Inc.) using conductive bottom layer B $35 \mu\text{m}$ thick, an insulator with relative permittivity $\epsilon_r = 4.9$ and 1.6 mm thick, inductive rectangular mesh layer S of conductive material $35 \mu\text{m}$ thick and a mesh lattice period of 5 mm with a lattice line 0.6 mm wide. The sheet was 95 mm square and we assumed no reflection at the sheet edge.

Figure 7 shows simulation results for electromagnetic fields induced around the 2DW sheet as electric field intensity in (a) and (b) showing that energy density decreases 30 dB by 3 mm from layer S. The decreasing

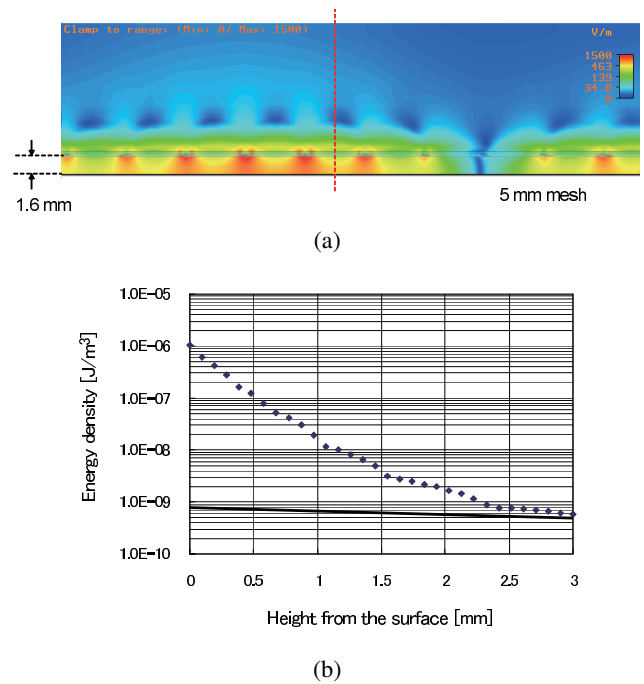


Fig. 7. Simulation results. (a) Electric field around 2DW sheet. (b) Plots of electromagnetic energy density along vertical dashed line above. Solid line: theoretical slope for attenuation coefficient 1.1 cm^{-1} .

curve is not purely exponential because horizontal mesh spacing d is comparable to the vertical observation range of 3 mm . Mesh pattern periodicity details the electromagnetic field as follows:

$$\begin{aligned}
 f(x, z) &= A \exp(-jkx) \left(\sum_{n=-\infty}^{\infty} B_n(z) \exp\left(j\frac{2\pi n}{d}x\right) \right) \\
 &\approx AC_0 \exp(-jkx) \exp(-k_1 z) \\
 &\quad + A \sum_{n \neq 0} C_n \exp\left(j\frac{2\pi n}{d}x\right) \exp\left(-\frac{2\pi n}{d}z\right),
 \end{aligned}$$

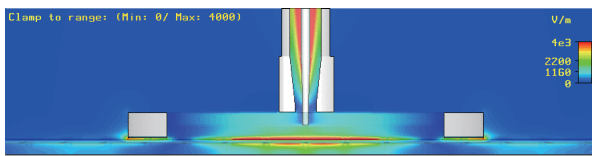
where $d \ll 2\pi/k$. (11)

Term

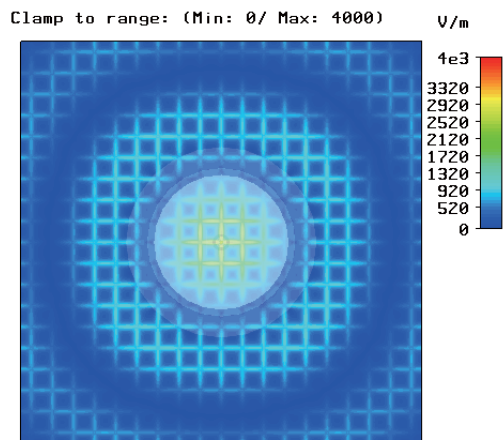
$$\sum_{n=-\infty}^{\infty} B_n \exp\left(j\frac{2\pi n}{d}x\right)$$

is the general expression of a function with period d . As Eq. (11) shows, the electric field around the sheet is a sum of multiple exponential curves along z with different attenuation lengths, thus the line in **Fig. 7(b)** is inflected several times when the major term in Eq. (11) switches. In Eq. (1) we omitted the term $n \neq 0$ by averaging the electromagnetic field in the mesh period. The term proportional to AC_0 in Eq. (11) corresponds to Eq. (1). The theoretical attenuation constant along z axis for $n = 0$ is equal to k_1 , or 1.1 cm^{-1} . Line of attenuation constant $k_1 = 1.1 \text{ cm}^{-1}$ is shown by the solid line in **Fig. 7(b)**. Note that the attenuation coefficient outside the graph ($z > 3 \text{ mm}$) is k_1 .

We also simulated the phenomenon in a nearfield cou-



(a)



(b)

Fig. 8. Simulation results. (a) Electric field intensity cross-section at the nearfield coupler and (b) top view.

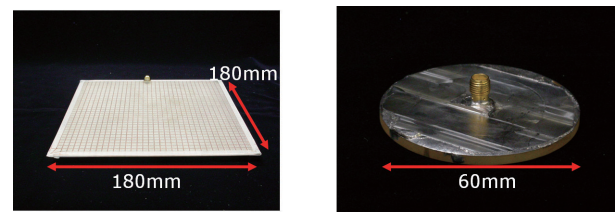
pler on the 2DW sheet, applying 2.4 GHz microwave through the SMA connector shown in **Fig. 8(a)**. Coupler dimensions are optimized so that it operates at 2.4 GHz. **Fig. 8(a)** shows an electric field in the coupler with $W = 5$ mm, $R = 17$ mm, and the other dimensions shown in **Fig. 6(a)**. **Fig. 8(b)** shows an overhead view of the electric field in the 2DW sheet. Applied energy is propagated concentrically in the sheet with the rectangular mesh layer.

4. Experiments

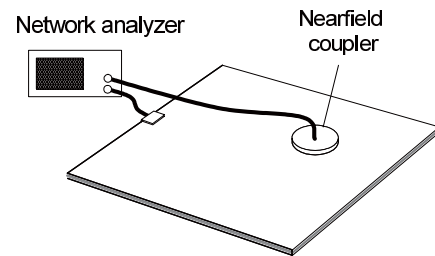
We fabricated a 180 mm square 2DW sheet with other parameters identical to those in the simulation and the nearfield coupler, prototype of **Fig. 6(a)** as shown in **Fig. 9**. Parameters R and W in **Fig. 6(a)** are 20 mm and 10 mm. The insulator between the sheet and coupler was paper 0.1 mm thick. The purpose of experiments is to confirm that sufficient power is transmitted from the sheet to the coupler on the sheet.

4.1. S-Parameter Observation

As shown in **Fig. 9**, the 2DW sheet has a subminiature version A (SMA) connector on the side edge connected to a 50Ω cable. Although some reflection occurs at the connection, we neglect this effect because our objective is to roughly estimate the connection between the coupler and sheet. One network analyzer port was connected to the 2DW sheet's connector and the other to the nearfield coupler and performance evaluated by measuring transmission coefficient S_{12} from 1 to 5 GHz.



(a)



(b)

Fig. 9. 2DW sheet used in experiment (left) and the nearfield coupler (right). The coupler is 60 mm in diameter for 2.4 GHz signals. Parameters R and W in **Fig. 6(a)** are set at 20 mm and 10 mm.

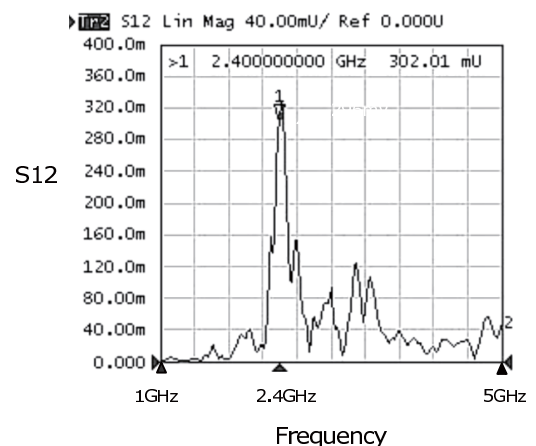


Fig. 10. Results for S_{12} measurement by a network analyzer. S_{12} is dimensionless, e.g., “240.0m” = $S_{12} = 0.24$. Transmission coefficient S_{12} was measured between the nearfield coupler and the SMA connector connected to the 2DW sheet. The definition of S_{12} is detailed in Section 4.

Figure 10 shows an example of measured $S_{12} = S_{21}$. Dimensionless parameter S_{12} mU at each frequency is the output signal amplitude received through the 50Ω cable connected to the 2DW sheet for the unit amplitude 1 U input signal applied to the nearfield coupler through the other 50Ω cable. The communication bandwidth is 300 MHz at 2.4 GHz, indicating that coupler resonance quality factor $Q = 8$ ($= 2.4/300$ MHz). Peak $S_{12} = 302$ mU = 0.302 at 2.4 GHz showing that 9% of input power was received by the other port at best.

We next looked at the relationship between the vertical distance above the sheet and S_{12} for 2.4 GHz, as shown in **Fig. 11(a)**. The proximity connection rapidly decreases for $d > 0.1$ mm. We also looked at the relationship be-

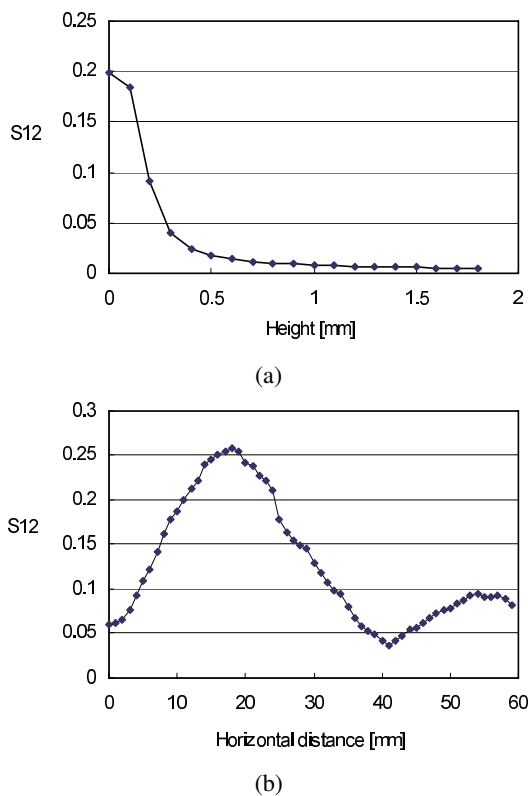


Fig. 11. Measured S_{12} versus coupler position. (a) S_{12} versus vertical coupler displacement and (b) S_{12} versus horizontal coupler displacement.

tween the horizontal sheet location and S_{12} , measuring S_{12} at 2.4 GHz moving the nearfield coupler horizontally straight on the sheet. As shown in **Fig. 11(b)**, S_{12} changed with the period of 4 cm reflecting the standing wave induced in the 2DW sheet. Data in **Fig. 10** is the result obtained at the peak of the standing wave.

4.2. Demonstration Experiments

Communication by IEEE 802.11b based on a 2.4 GHz signal was demonstrated in an experiment in which a personal computer transmitted a video signal to another PC using commercially available wireless LAN cards whose antennas were replaced by nearfield couplers – the only difference from conventional wireless peer-to-peer communication, as shown in **Fig. 12(a)**. Good signal transmission was possible through the 2DW sheet and two nearfield couplers. Since the 2DW sheet size was finite, standing waves induced in the sheet degrade communication quality, but the adverse effect was negligible in 11 Mbps connection.

We also confirmed experimentally that a LED and a small motor operated on the power caught by nearfield couplers as shown in **Figs. 12(b)** and **(c)**. We supplied 2 W microwaves at 2.4 GHz to the 2DW sheet, and the electromagnetic wave the coupler caught was rectified by a full-wave rectifying circuit as shown in **Fig. 12(d)**. More efficient rectifying circuits are studied in [9], for example. The LED brightness and the motor rotation depended on

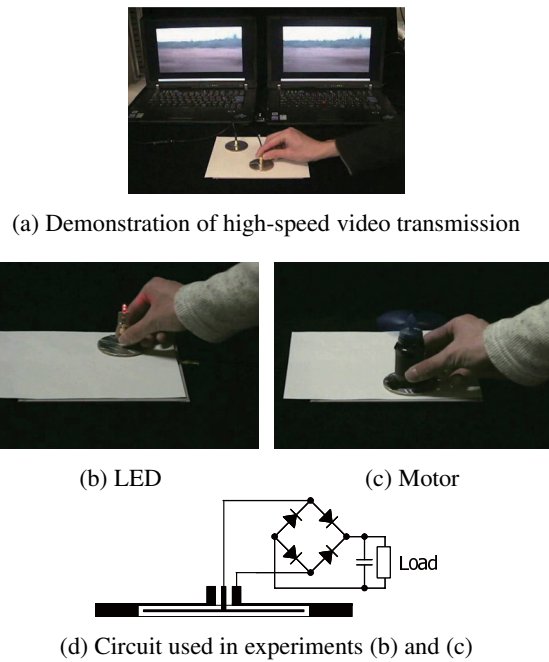


Fig. 12. Views of demonstrations. (a) Movie transmission using IEEE 802.11b. The PC at left plays a video transmitting the video signal to the next computer. (b) and (c) Power transmission to a LED and a motor. (d) Full-wave rectifying circuit for power reception.

the location in the 2DW sheet, which was due to the standing wave in the sheet. For a 50 Ω resistor as the load in **Fig. 12(d)**, instead of the LED or the motor, the maximum consumed power was measured to be 80 mW for 2 W microwave input.

5. Conclusions

We have proposed a 2D power supply based on a proximity (nearfield) connection, analyzing and simulating signal transmission through a mesh 2DW sheet to clarify an evanescent wave trapped at the sheet propagating over the sheet. We fabricated prototypes of a nearfield coupler and a 180 mm \times 180 mm 2DW sheet based on numerical simulations and evaluated their performance. We confirmed experimentally that the coupler’s communication bandwidth is 300 MHz at 2.4 GHz and 9% of power supplied to the 2DW sheet was absorbed at best by the nearfield coupler through the sheet. In the experiment we input 2 W into the 2DW sheet, a load connected to a single coupler could consume 80 mW DC power. Through this study, we thus showed that 2D power transmission and communication are feasible. Increasing transmission efficiency and decreasing electromagnetic radiation into the atmosphere are the next technical challenges we face.

Acknowledgements

We thank Cellcross Co. Ltd.' Dr. Naoya Asamura, Dr. Mitsuhiro Hakozaki, and Tetsuro Kiyomatsu for their advice and cooperation in device fabrication.

References:

- [1] H. Ishihara and T. Fukuda, "Micro Autonomous Robotic System," J. of Robotics and Mechatronics, Vol.11, No.5, pp. 443-447, 1999.
- [2] T. Sekitani, M. Takamiya, Y. Noguchi, S. Nakano, Y. Kato, T. Sakurai, and T. Someya, "A large-area wireless power-transmission sheet using printed organic transistors and plastic MEMS switches," Nature Materials, Vol.6, pp. 413-417, 2007.
- [3] N. Shinohara, H. Matsumoto, and K. Hashimoto, "Solar Power Station/Satellite (SPS) with Phase Controlled Magnetrons," IEICE Trans. Electron, Vol.E86-C, No.8, pp. 1550-1555, 2003.
- [4] A. Karalis, J. D. Joannopoulos, and M. Soljačić, "Efficient wireless non-radiative mid-range energy transfer," Annals of Physics, Vol.323, No.1, pp. 34-48, 2008.
- [5] N. Yamahira, Y. Makino, H. Itai, and H. Shinoda, "Proximity Connection in Two-Dimensional Signal Transmission," Proc. SICE-ICASE Int. Joint Conf. 2006, Oct., Busan, Korea, pp. 2735-2740, 2006.
- [6] A. Noda and H. Shinoda, "Power Transmission Coupler for Low Leakage 2D-Communication Sheet," Proc. INSS2009, Pittsburgh, June 17-19, pp. 24-30, 2009.
- [7] Y. Monnai and H. Shinoda, "Converting 2D Microwave into 3D Beam Using Dielectric Grating Antenna," Proc. INSS2009, Pittsburgh, June 17-19, pp. 183-187, 2009.
- [8] J. D. Kraus and D. A. Fleisch, "Electromagnetics with Applications, 5th Edition," McGraw-Hill, pp. 480-487, 1999.
- [9] T. Miura, N. Shinohara, and H. Matsumoto, "Experimental Study of Rectenna Connection for Microwave Power Transmission," Electronics and Communications in Japan, Part2, Vol.84, No.2, pp. 27-36, 2001.



Name:
Hiroaki Shinoda

Affiliation:
Associate Professor, Department of Information Physics and Computing, Graduate School of Information Science and Technology, The University of Tokyo

Address:

7-3-1 Hongo, Bunkyo-ku, Tokyo 113-8656, Japan

Brief Biographical History:

1995- Lecturer, Tokyo University of Agriculture and Technology
1997- Associate Professor, Tokyo University of Agriculture and Technology
1999- Visiting Researcher, UC Berkeley
2000-Associate Professor, The University of Tokyo

Main Works:

• Information physics, tactile/haptic interfaces, sensor systems and devices, sensor networks, two-dimensional communication, human interfaces, and optical/acoustic measurement.

Membership in Academic Societies:

- The Society of Instrument and Control Engineers (SICE)
- The Japan Society of Mechanical Engineers (JSME)
- The Institute of Electrical Engineers of Japan (IEEJ)
- The Robotics Society of Japan (RSJ)
- The Virtual Reality Society of Japan (VRSJ)
- The Institute of Electrical and Electronics Engineers (IEEE)



Name:
Yasutoshi Makino

Affiliation:
Keio University

Address:

4-1-1 Hiyoshi, Kohoku-ku, Yokohama-shi, Kanagawa 223-8526, Japan

Brief Biographical History:

2007- Received Ph.D. degree of Information Science and Technology from The University of Tokyo
2008- Researcher in The University of Tokyo
2009- Assistant Professor in Keio University

Main Works:

• Y. Makino and H. Shinoda, "Myoelectric Pattern Measurement Based on Two-Dimensional Communication Technology," Proc. SICE Annual Conf. 2007, pp. 2145-2149, 2007.

Membership in Academic Societies:

- The Society of Instrument and Control Engineers (SICE)



Name:
Naoshi Yamahira

Affiliation:
Research Engineer, Steel Research Laboratory

Address:

1-1 Minamiwatarida-cho, Kawasaki-ku, Kawasaki-shi, Kanagawa 210-0855, Japan

Brief Biographical History:

2008- Joined JFE Steel Corp.

Main Works:

• "Proximity Connection in Two-Dimensional Signal Transmission," Proc. SICE-ICASE Int. Joint Conf. 2006, pp. 2005-2009, Oct. 2006.



Name:
Hiroto Itai

Affiliation:
Senior Researcher, Research Department, Cellcross Co.,Ltd.

Address:

Entrepreneur Plaza 204, 7-3-1, Hongo, Bunkyo-ku, Tokyo 113-0033, Japan

Brief Biographical History:

2004- Joined Cellcross Co.,Ltd.

Main Works:

• "Interactive Window Based on 2D Communication Technology: Integrating Ubiquitous Devices on Transparent Medium," Pervasive 2009, pp. 193-196, May 2009

Membership in Academic Societies:

- The Society of Instrument and Control Engineers (SICE)